Geophysical Prospecting, 2003, **51**, 393–408

Use of VFSA for resolution, sensitivity and uncertainty analysis in 1D DC resistivity and IP inversion

Bimalendu B. Bhattacharya,[1]* Shalivahan[1] and Mrinal K. Sen[2]

[1]*Department of Applied Geophysics, Indian School of Mines, Dhanbad 826004, India, and* [2]*Institute for Geophysics, The University of Texas at Austin, Austin, TX 78759-8500, USA*

Received March 2001, revision accepted January 2003

ABSTRACT

We present results from the resolution and sensitivity analysis of 1D DC resistivity and IP sounding data using a non-linear inversion. The inversion scheme uses a theoretically correct Metropolis–Gibbs' sampling technique and an approximate method using numerous models sampled by a global optimization algorithm called very fast simulated annealing (VFSA). VFSA has recently been found to be computationally efficient in several geophysical parameter estimation problems. Unlike conventional simulated annealing (SA), in VFSA the perturbations are generated from the model parameters according to a Cauchy-like distribution whose shape changes with each iteration. This results in an algorithm that converges much faster than a standard SA. In the course of finding the optimal solution, VFSA samples several models from the search space. All these models can be used to obtain estimates of uncertainty in the derived solution. This method makes no assumptions about the shape of an *a posteriori* probability density function in the model space. Here, we carry out a VFSA-based sensitivity analysis with several synthetic and field sounding data sets for resistivity and IP. The resolution capability of the VFSA algorithm as seen from the sensitivity analysis is satisfactory. The interpretation of VES and IP sounding data by VFSA, incorporating resolution, sensitivity and uncertainty of layer parameters, would generally be more useful than the conventional best-fit techniques.

INTRODUCTION

Induced polarization (IP) and resistivity sounding data are collected in a routine manner for groundwater exploration, especially over sedimentary formations. This method is also used over porphyry-type ore deposits. IP data are also collected in environmental surveys (Barker 1990). Compilations of IP work have been given by Bertin and Loeb (1976), Sumner (1976), Fink *et al*. (1990) and Ward (1990). Patella (1975) obtained an expression for apparent chargeability (m_a) in different stratigraphic situations with time-domain IP soundings using a Schlumberger array. Dixon and Doherty (1977) suggested two methods for calculating chargeability over a layered earth using a Schlumberger array. The calculation of apparent resistivity over a multilayered earth became quite simple, due to the application of filter theory to the interpretation of vertical electrical sounding (VES) data (Ghosh 1970, 1971a,b).

The inversion of resistivity data has been carried out by various workers (e.g. Inman, Ryu and Ward 1973; Inman 1975; Tripp, Hohmann and Swift 1984; Bhattacharya and Ghosh Roy 1988; Shima 1990; Narayan and Dusseault 1992; Narayan, Dusseault and Nobes 1994, and others). Fitting the field data to the calculated resistivity values is generally carried out in a least-squares sense. The least-squares fitting is performed on a linearized version of the governing equation, although the governing equation of apparent resistivity over a layered earth is a non-linear equation. The solution depends on the choice of starting model. Linearized inversion

*E-mail: bbb@perl.ism.ac.in

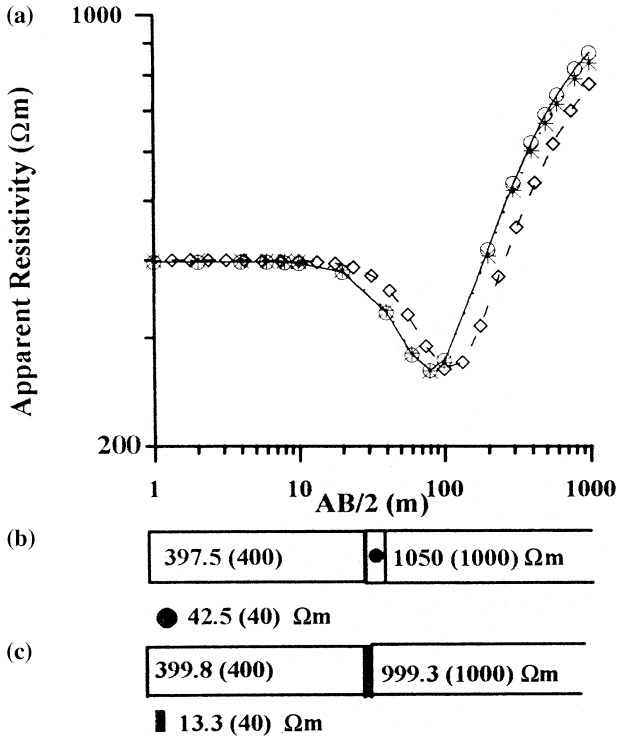

Figure 1 (a) Synthetic (✳), computed VFSA (○) and linear (□) VES curves for a three-layer model with a 10-m layer occurring at a depth of 30 m; (b) VFSA model; (c) model from linear inversion. The numbers in parentheses are the actual resistivity values of the assumed model.

methods generally find a minimum in the close neighbourhood of the starting solution. In situations where the error function may have several minima, it is necessary either to start very close to the global minimum or to try several starting points, in the hope that one of them will lead to the best solution. Almost all linear inversion schemes are deterministic algorithms. They use local properties of the misfit function to calculate an update of the current solution and search in the downhill direction. Since it searches only in the downhill direction, the convergence is very fast. These methods may not be able to reach the global minimum if the starting solution is nearer to one of the local minima than the global minimum. Basically, non-linear inverse problems are usually solved with linearized techniques that depend heavily on the accuracy of the initial estimates of the model parameters. With linearization, objective functions can be minimized efficiently, but the risk of local rather than global optimization can be severe (Rothman 1985; Sen, Bhattacharya and Stoffa 1993). We address the problem encountered in the non-linear inversion of resistivity and IP data, when no *a priori* information on the model parameters is available and no good initial guess can be made. The large number of iterations becomes necessary in non-linear inversion as it searches in both the uphill and downhill directions in order to determine the global minimum. In addition we also address the issue of uniqueness by estimating different measures of uncertainty. Usually in a local optimization, the curvature of the error surface of the best-fit model is used to estimate variances in the resulting solution (Menke 1984). The basic assumption here is that the *a posteriori* distribution is Gaussian. The same procedure can be employed with the best-fit model obtained by a single run of a global optimization method such as very fast simulated annealing (VFSA). However, a Metropolis–Gibbs' sampling approach (Mosegaard and Tarantola 1995; Sen and Stoffa 1995) samples models from the *a posteriori* distribution and makes no assumption on the shape of the *a posteriori* probability distribution. We follow this approach in the estimation of uncertainties.

Time-domain IP data inversions were carried out by Pelton, Rijo and Swift (1978), Sasaki (1982) and Rijo (1984). La Brecque (1991) carried out 2D inversion of IP data for cross-hole tomography. Beard and Hohmann (1992) suggested 3D inversion of IP data for small resistivity contrasts. Oldenburg and Li (1994) illustrated IP inversion results over a 2D earth structure and field results using inversion of dipole–dipole data. Oldenburg, Li and Ellis (1997) inverted magnetic, DC resistivity, IP and airborne electromagnetic (EM) data from a copper–gold porphyry deposit. Beard, Hohmann and Tripp (1996) achieved a fast forward solution, accurate at low resistivity contrasts, and made use of it in resistivity/IP inversion for dipole–dipole pseudosections. Esparza and Gomez-Trevino (1997) suggested 1D inversion of resistivity and IP sounding data for layered earth models. Their models have the minimum number of layers required to fit a resistivity sounding curve or a combined resistivity and IP sounding curve. We describe the application of a non-linear optimization algorithm, known as very fast simulated annealing (VFSA), in the estimation of earth model parameters from 1D VES and IP sounding data. We focus not only on obtaining a best-fit model but also on deriving the associated uncertainties in the obtained solution.

FORWARD MODELLING

Apparent resistivity

The apparent resistivity of a multilayered earth model for a Schlumberger array λ is given by (Koefoed 1979)

$$\rho_{aS} = r^2 \int_0^\infty T(\lambda) J_1(\lambda r)\, \lambda\, d\lambda, \tag{1}$$

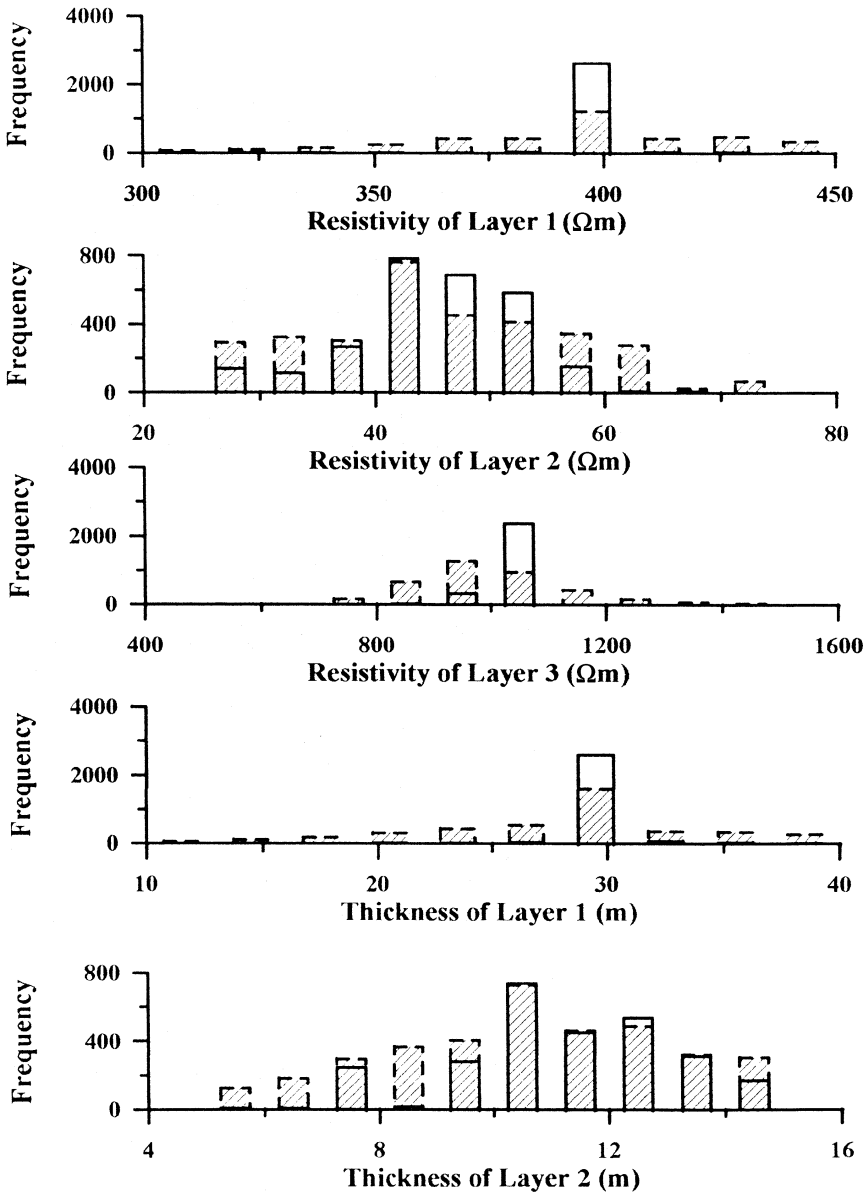

Figure 2 Histograms of the model parameters of the synthetic VES curve for VFSA inversion (Fig. 1), sampled at 10 000 iterations. The shaded columns with dashed boundaries are for the same synthetic VES curve (Fig. 1) with 10% Gaussian random noise added to each data sample.

where $2r$ is the current electrode spacing $AB(r = AB/2)$, ρ_{aS} is the Schlumberger apparent resistivity, $T(\lambda)$ is the resistivity transform, J_1 is the Bessel function of the first order and λ is the integration factor. $T(\lambda) = \rho_1\{1 + 2\theta_1(\lambda)\}$ where $\theta_1(\lambda)$ is the kernel function, which is controlled by the resistivities and thicknesses of the layers and ρ_1 is the first-layer resistivity. The forward resistivity problem uses the linear-filter method proposed by Ghosh (1970, 1971b). The computation of an apparent-resistivity curve using linear-filter theory is executed in two steps. In the first step, the sample value of the resistivity transform from the layer parameters is computed. The next step is to determine the sample values of the apparent resistivity from those of the resistivity transform using a linear filter. Mathematically, the linear-filter operation is defined as (Koefoed 1979)

$$\rho_{aS}(x_o) = \sum_j f_j T(y_o - j\Delta y), \tag{2}$$

where x_o is the abscissa of the point of the output function (apparent resistivity), y_o is the abscissa of the first point of the input function (resistivity transform), Δy is the sampling interval and f_j are the filter coefficients by which the sample values of the resistivity transform are multiplied to obtain the apparent resistivity.

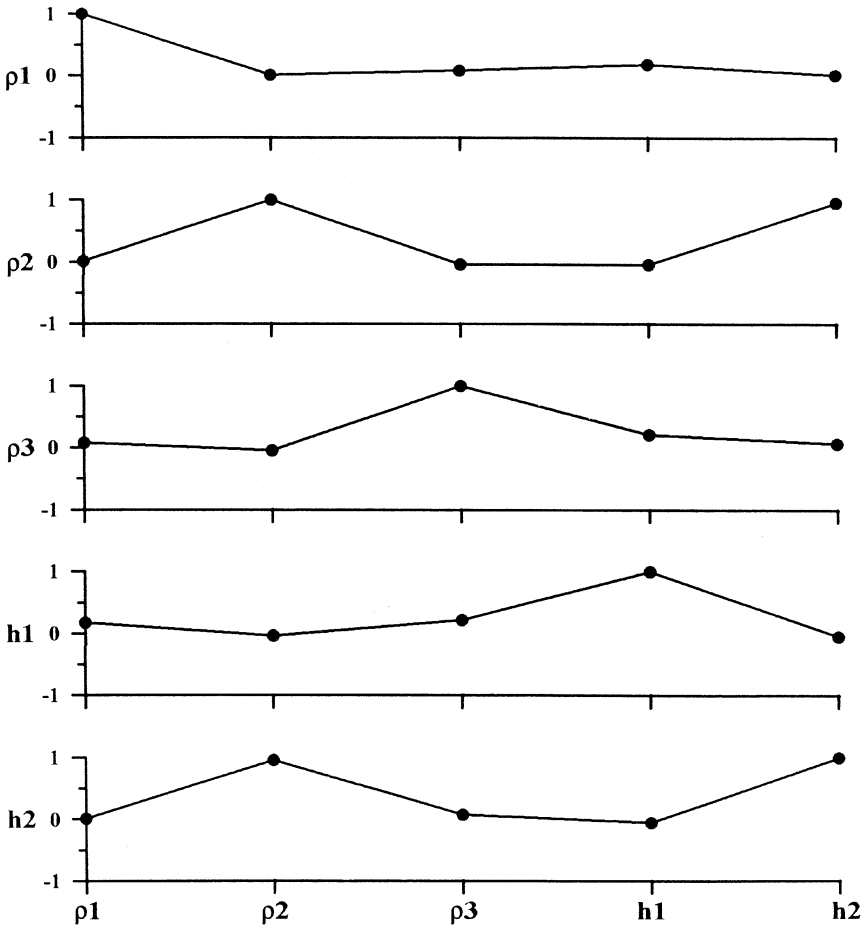

Figure 3 *A posteriori* correlation matrix for the synthetic VES curve (Fig. 1).

APPARENT CHARGEABILITY

We now consider a layered earth with layers having resistivities ρ_i $(i = 1, \ldots, n)$ and thicknesses h_j $(j = 1, \ldots, n-1)$, and thus the apparent resistivity is given by

$$\rho_a = f(\rho_i, h_j)$$

for a given electrode spacing. If these layers also show chargeabilities m_i $(0 < m_i < 1)$, then according to Seigel (1959), the resistivities of the layers change to

$$\rho_i^* = (\rho_i/(1 - m_i)),$$

and the new apparent resistivity over such a layered earth for the same spacing is $\rho_a^* = f(\rho_i^*, h_j)$. The apparent chargeability m_a for such a layered earth is given by

$$m_a = \left(\rho_a^* - \rho_a\right)/\rho_a^*. \quad (3)$$

Therefore, the calculation of the apparent chargeability for a Schlumberger array can be obtained by using the standard filter coefficients used for VES with Schlumberger arrays for both cases, i.e. ρ_a^* and ρ_a, where ρ_a^* is calculated for all electrode spacings.

SIMULATED ANNEALING AND VERY FAST SIMULATED ANNEALING

Accounts of simulated annealing (SA) and genetic algorithms (GA) for geophysical applications have been given by Sen and Stoffa (1995). The SA method has been used in the inversion of resistivity data by Bhattacharya *et al.* (1992, paper presented at International Conference on Mathematical Modelling and Computer Simulation), Sen *et al.* (1993) and Chunduru *et al.* (1995, 1996). Unlike the GA that imitates the processes of biological evolution, the annealing process means that a solid in a heat bath is initially heated by increasing the temperature and is then cooled slowly so that the particles arrange themselves in a low-energy ground state where

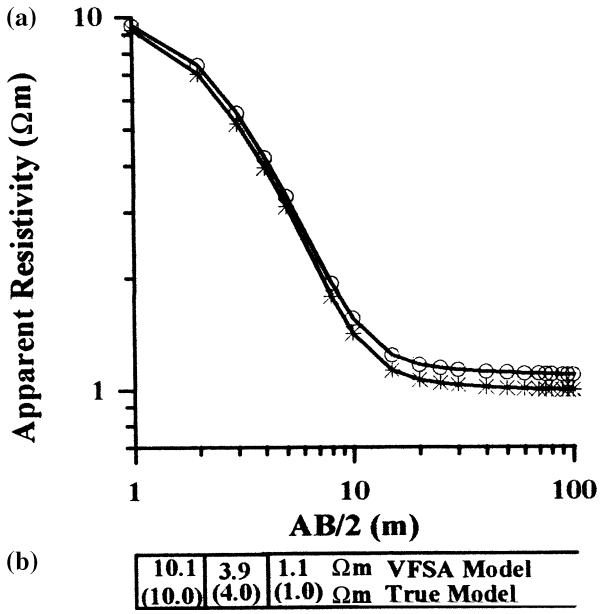

Figure 4 (a) Synthetic (✳) and computed (○) VES curves with 10% Gaussian random noise added to each data sample; (b) VFSA model. The numbers in parentheses are the actual resistivity values of the assumed model. The thicknesses of the layers are the same in both cases.

crystallization occurs. The formation of the crystal is analogous to reaching the global minimum energy in an optimization problem. The SA method has been used in multiparameter optimization problems by many workers (Rothman 1985; Sen and Stoffa 1991; Normark and Mosegaard 1993). Ingber (1989) gave a detailed description of various SA methods. A brief summary of SA and VFSA is presented here for completeness as well as for its application to the problem. The advantages of optimization using SA are: (i) computations of derivatives are not required; (ii) inversion of large matrices is not required; (iii) the starting model need not be close to the global minimum, which can be of great help in many real earth problems; (iv) computer coding of the algorithm is quite simple; (v) most of the SA methods find an optimal solution. Many gradient descent methods require the computation of a derivative matrix and the generation of products of matrices. Although for 1D resistivity and IP methods the gradient methods can be computed analytically, generation of the products of matrices such as GTG (G is forward modelling operator) may require numerous floating-point multiplication and addition operations. In other words, a single iteration of a gradient descent algorithm involves much more computation than a single forward model evaluation.

Simulated annealing (SA)

Metropolis *et al.* (1953) introduced an algorithm that is essentially a two-step procedure. In it, a model is drawn at random, say $\mathbf{m}_i$, and then a decision is made whether to accept or reject it. Data are generated, using the forward problem, for this model. The error (also termed energy) $E(\mathbf{m}_i)$ for this model is computed using the equation,

$$E(\mathbf{m}_i) = \frac{1}{N}\sum_{i=1}^{N}\left(\mathbf{r}_c^i - \mathbf{r}_o^i\right)^2, \tag{4}$$

where $\mathbf{r}_c$ and $\mathbf{r}_o$ are the calculated and observed data vectors, respectively. Here, N is the length of the data vector, which is the number of observation points. For each parameter we define a search limit $\mathbf{m}_i^{\min} \leq \mathbf{m}_i \leq \mathbf{m}_i^{\max}$ and $\mathbf{m}_i$ is perturbed to obtain a new model $\mathbf{m}_j = \mathbf{m}_i + \Delta\mathbf{m}_i$ with error $E(\mathbf{m}_j)$. The search increment $\Delta\mathbf{m}_i$ defines the model resolution desired. In a Metropolis SA, $\Delta\mathbf{m}_i$ is chosen continuously within the search window. However, in a heat-bath SA, it is chosen so as not to make the computations prohibitively expensive (Sen *et al.* 1993). The search limit and search increment are usually different for different model parameters and are chosen so as not to make the computation prohibitively expensive. The change in energy is given by

$$\Delta E_{ij} = E(\mathbf{m}_j) - E(\mathbf{m}_i),$$

and if $\Delta E_{ij} \leq 0$, $\mathbf{m}_j$ is accepted. If $\Delta E > 0$, then the new model is accepted with a probability,

$$P = \exp(-\Delta E_{ij}/T),$$

where T is the control parameter, called the temperature. This generation-acceptance process is repeated a number of times for a given temperature. The temperature is then reduced following a cooling schedule and the process is repeated until convergence is reached. The convergence in this case is achieved when the error does not change for several iterations.

Very fast simulated annealing (VFSA)

For this case, the model is drawn from a Cauchy or Cauchy-like distribution that is a function of temperature (Ingber 1989). The advantage in this case is that, at high temperatures, the algorithm allows for searches far beyond the current position. At lower temperatures, however, it searches for improvement in the close neighbourhood of the current model. The acceptance criterion of the algorithm is the same as that used in SA. The salient features of VFSA are that (i) it requires a temperature for each model parameter and these can

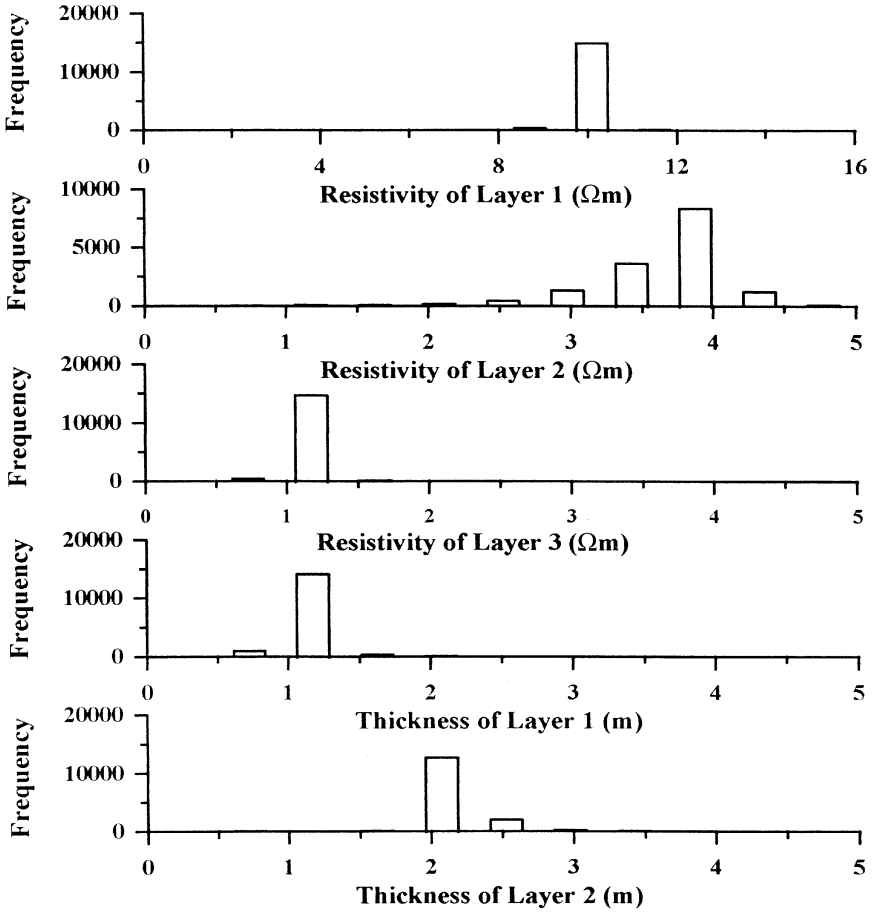

Figure 5 Histograms of the model parameters of the synthetic VES curve with 10% Gaussian random noise added for VFSA inversion (Fig. 4), sampled at 10 000 iterations.

be different for different model parameters, and (ii) it requires a temperature to be used in the acceptance criterion, which may be different from the model parameter temperatures. Ingber (1989) showed that for such a distribution the global minimum can be obtained statistically by using the much faster cooling schedule given by

$$T_i(k) = T_{0i}\exp\left(-c_i k^{1/NM}\right), \tag{5}$$

where $T_i(k)$ is the temperature at iteration k, T_{0i} is the initial temperature for model parameter i, c_i is the parameter used to control the temperature schedule and help tune the algorithm for specific problems, and NM is the number of model parameters. It is sensible to choose control over c_i, such that

$$T_{fi} = T_{0i}\exp(-m_i), \tag{6}$$

where the final iteration, $k_f = \exp n_i$ and T_{fi} is the final temperature as desired for model parameter i (Ingber 1989; Ingber and Rosen 1992). Thus,

$$c_i = m_i\exp(-n_i/NM). \tag{7}$$

INVERSION OF VES AND IP SOUNDING DATA

In our application of the method to VES and IP sounding data, we attempt to determine the values of the chargeabilities, resistivities and thicknesses of a multilayered earth, assuming variation in depth only. The same algorithm is used for IP inversion as for resistivity inversion. For an n-layer earth model, the total number of parameters for IP sounding is $3n - 1$. However, for a layered earth without any polarizability of layers, the number of sounding parameters will be $2n - 1$ only. The apparent chargeability (m_a) data are inverted to determine the values of m_i, ρ_i and h_i. Apparent-resistivity (ρ_a^*) data are also inverted to obtain ρ_i^* and h_i. Using the relationship $\rho_i^* = \rho_i/(1 - m_i)$, ρ_i is once again obtained from apparent-resistivity inversion. The parameters ρ_i and h_i are cross-checked, using both the inversions. In our VFSA inversion we use an objective function defined in (4).

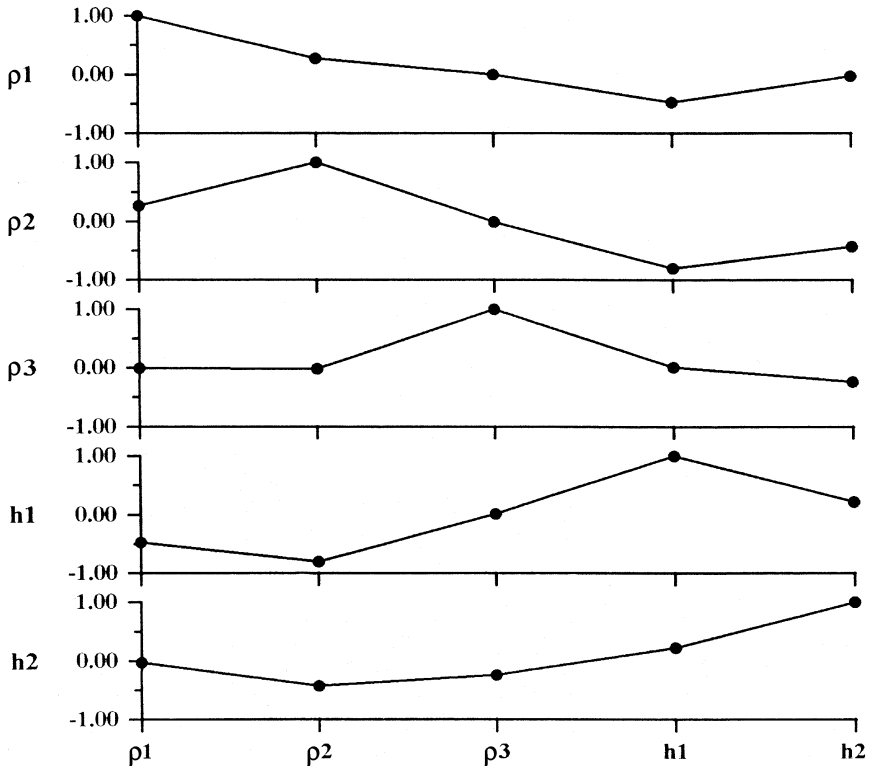

Figure 6 *A posteriori* correlation matrix for the synthetic VES curve with 10% Gaussian random noise added (Fig. 4).

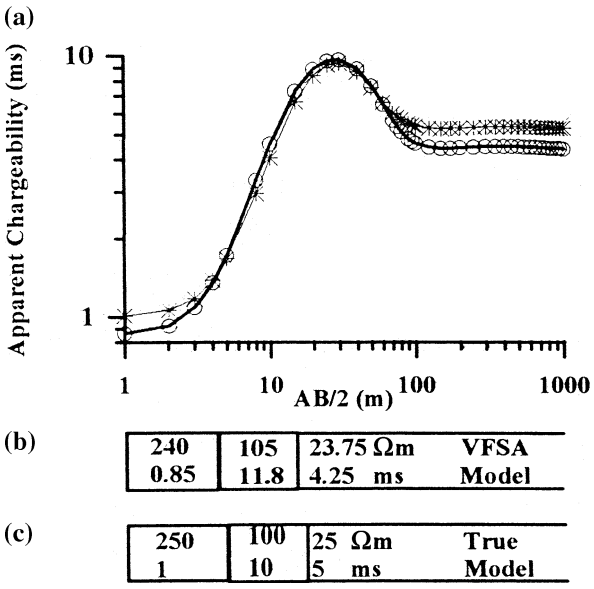

Figure 7 (a) Synthetic (⋇) and computed (○) IP curves; (b) VFSA model; (c) true model.

THE SENSITIVITY AND RESOLUTION ANALYSIS

It is quite well known that the resistivity inverse problem is generally ill-posed and non-unique estimates of model parameters are obtained. There are essentially two approaches to dealing with non-uniqueness. One is to parametrize the earth model by a large number of layers (cells in 2D or 3D) and to generate smooth images of the subsurface. The second approach is to use *a priori* information of parameters (bounds, means, probability laws), which may be entered in the optimization process. We take the latter approach since an experienced interpreter normally has a fairly good knowledge of the geology and can make an intelligent guess at the number of possible layers. We do note that such a parametrization introduces a bias into our final result but in such a situation we rely on the skill of the interpreters. Given this parametrization, we use VFSA to find a model (or models) that produces an acceptable fit to the data. We also note that VFSA can be run with large numbers of layers with an objective function that includes a model norm. The model norm can take any of the L_p-norms where we have a two-part objective function, one for data fitting and the other for model constraints. The model norm can also be designed to impose constraints. In the Bayesian description of the inverse problem as used here in the context of uncertainty analysis, the models are drawn from a suitably defined prior ensemble. Even with sparse parametrization, non-uniqueness plays an important role. In particular in the case of geoelectric sounding, we may be able to fit a range of models that may explain the data equally

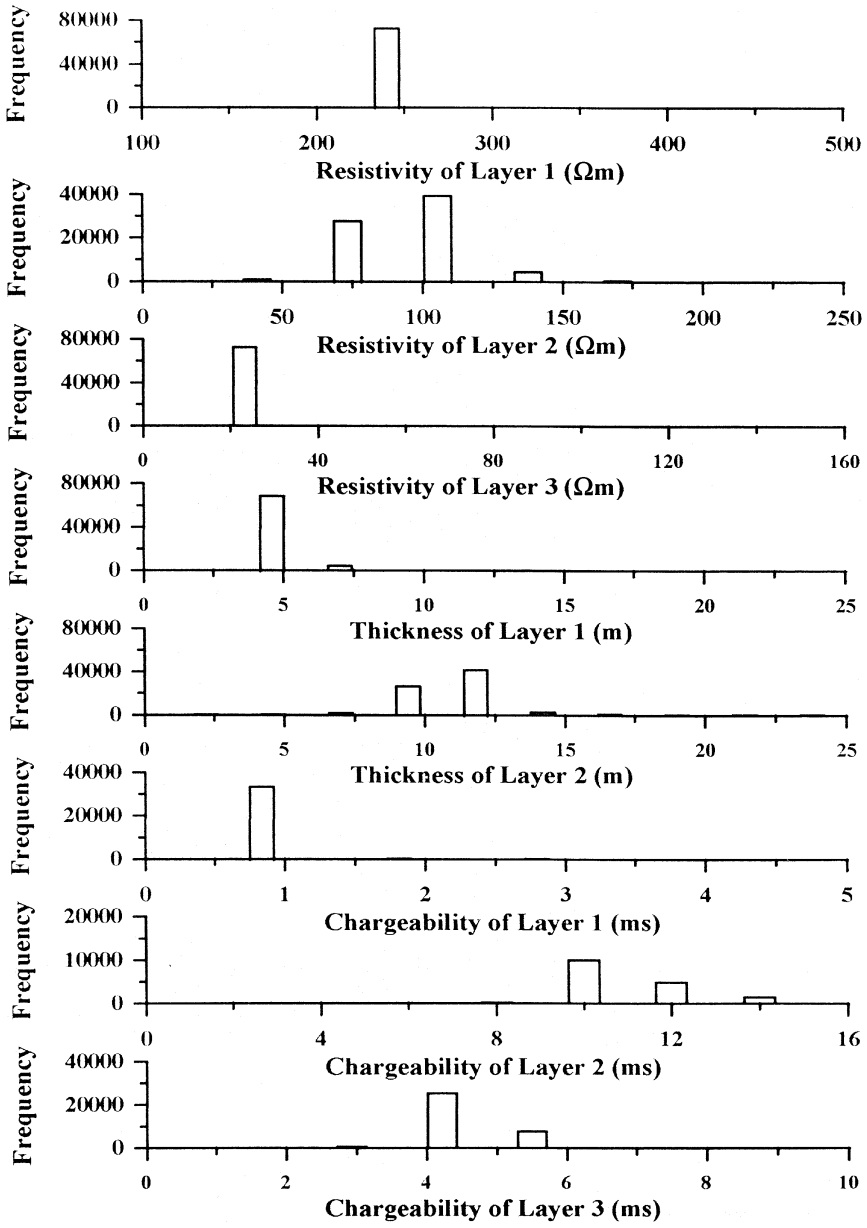

Figure 8 Histograms of the model parameters of the synthetic IP curve for VFSA inversion (Fig. 7), sampled at 10 000 iterations.

well. There may also be a trade-off between different model parameters. Thus in addition to fitting the data with synthetics, we also aim at estimating uncertainties in our derived solution. A large number of models sampled by VFSA can be used to study the sensitivity and resolution of the model parameters. Essentially we can make estimates of a mean model, *a posteriori* model covariances and any higher-order moments to characterize uncertainty. Theoretically correct estimates of uncertainty can only be made by use of a computationally intensive Metropolis–Gibbs' sampling approach. However, Sen and Stoffa (1995) showed that the models sampled by multiple VFSA runs can be used to obtain a fairly good estimate of uncertainty. Note that a VFSA-based method makes no assumption on the shape of the *a posteriori* probability density function in model space.

In essence, we use all the models accepted by VFSA to generate histograms for all the layer parameters, in order to study their resolutions and accuracy. To understand the interdependence between different model parameters, the *a posteriori* correlation matrices are studied. In our application we found it adequate to use 20 multiple VFSA runs with 10 000 iterations at a constant acceptance temperature (T) of 1.0.

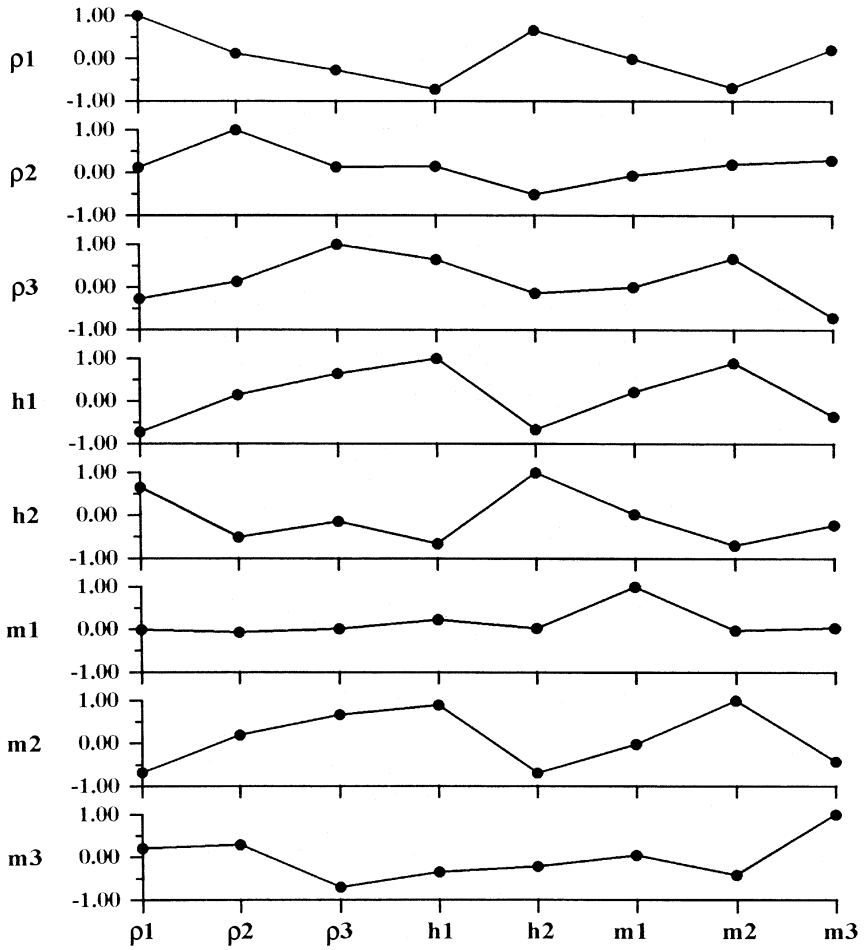

Figure 9 *A posteriori* correlation matrix for the synthetic IP curve (Fig. 7).

The *a posteriori* correlation matrix is an indication of the linear dependence between the parameters. The elements of the correlation matrix are given by (Jenkins and Watts 1968)

$$[\mathrm{cor}(\mathbf{P})]_{ij} = \frac{[\mathrm{cov}(\mathbf{P})]_{ij}}{[\mathrm{cov}(\mathbf{P})]_{ii}^{1/2}[\mathrm{cov}(\mathbf{P})]_{jj}^{1/2}}.$$

If the value of $[\mathrm{cor}(\mathbf{P})]_{ij}$ is near unity, then the parameters P_i and P_j are strongly correlated and nearly linearly dependent.

The covariance of P is given by

$$\mathbf{P} = \sum (\mathbf{m} - \langle \mathbf{m} \rangle)(\mathbf{m} - \langle \mathbf{m} \rangle)^{\mathrm{T}} \sigma(\mathbf{m}),$$

where

$$\langle \mathbf{m} \rangle = \sum \mathbf{m} \sigma(\mathbf{m}).$$

EXAMPLES OF SENSITIVITY AND RESOLUTION ANALYSIS

Synthetic VES and IP sounding data

Here we present the sensitivity and resolution analysis of two VES data sets, with and without noise, and one IP sounding data set.

VES data without noise

For this case we generated a synthetic VES curve for a three-layer earth model (H-type) to find out how well a 10-m layer at 30 m depth is really resolved by the VFSA inversion algorithm. The two layers, which overlie a basement of 1000 Ωm resistivity, have resistivities of 400 Ωm and 40 Ωm. The search window and search increments for the layer parameters are shown in Table 1. The synthetic and the computed curves are practically coincident and are shown by asterisks (⋇)

Table 1 Search window and search increments for the layer parameters of the synthetic model

Layers	ρ_{min} (Ωm)	ρ_{max} (Ωm)	$\Delta\rho$ (Ωm)	h_{min} (m)	h_{max} (m)	Δh (m)
1	300	450	10	10	40	1
2	25	75	1	5	15	1
3	500	1500	100	–	–	–

and open circles (○), respectively, in Fig. 1(a). The VES curve has also been interpreted by linear inversion and is shown by broken lines (- - -) with data points (□) (Patra and Nath 1998), for comparison with VFSA, with the initial guess for all the parameters reduced by 10% from the actual value. If the search window is taken much wider, the model space is large, and then VFSA also attains the global minimum but with more computer time. The model obtained from the linear inversion is shown in Fig. 1(c) with the actual values shown in parentheses. The parameters obtained from the final VFSA model (Fig. 1b) are much closer to the actual values for the second layer with a much wider search limit compared with linear inversion with a much closer initial guess. Hohmann and Raiche (1987) studied a similar model with a 10-m thick highly conducting (0.25 Ωm) layer occurring at a depth of 30 m. Resistivity inversion was able to resolve the longitudinal conductance (h_2/ρ_2) of this layer, but the individual estimates of ρ_2 and h_2 are out by a factor of four. Joint inversion of transient EM and resistivity soundings carried out by Hohmann and Raiche (1987) shows quite good individual estimates for ρ_2 and h_2. The linear inversion carried out for our model shows that only the longitudinal conductance is resolved. The individual estimates of ρ_2 and h_2 are out by a factor of one-fourth. It is interesting to note that the individual estimates of ρ_2 and h_2 with VFSA inversion are quite good and are similar to the joint inversion results obtained by Hohmann and Raiche (1987). Figure 2 shows the histograms (Rothman 1985; Tarantola 1987; Sen and Stoffa 1995) of the model parameters sampled over the 10 000 iterations for VFSA. The histograms show that ρ_1, ρ_3 and h_1 are very well resolved, but this is not the case for ρ_2 and h_2. The *a posteriori* correlation matrix (Jenkins and Watts 1968) (Fig. 3) helps in understanding the interdependence between different model parameters. There is a strong positive correlation between ρ_2 and h_2. This means that if ρ_2 and h_2 are both increased or decreased, the apparent-resistivity curve will not change. Thus, even though a single VFSA inversion appears to converge to the true values of ρ_2 and h_2, the trade-off between these two parameters is apparent in their correlation value. The histograms for ρ_2 and h_2 show a larger

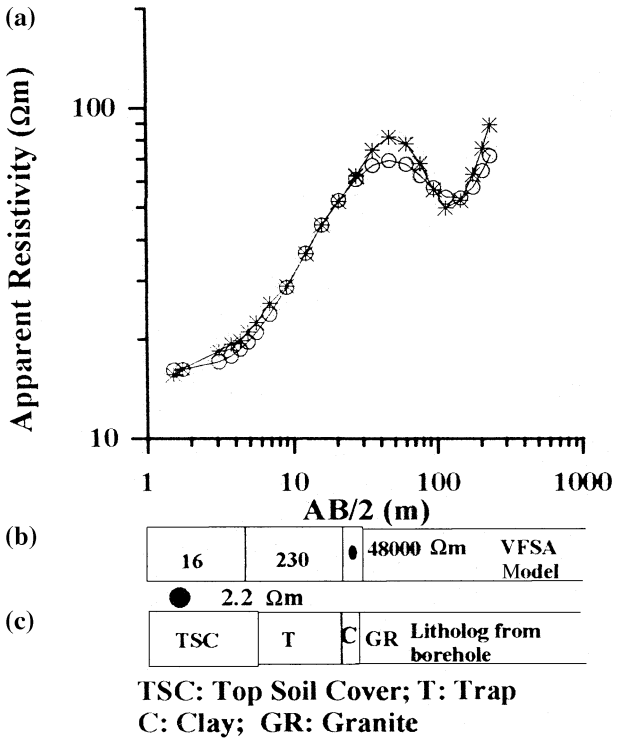

Figure 10 (a) Field (⊛) and computed (○) VES curves; (b) VFSA model; (c) lithology from borehole section.

spread. Figure 2 also shows the histograms (shown by shaded columns with dashed boundaries) for 10% Gaussian random noise added to each data sample for the same VES curve. It can be seen that the histogram pattern for both cases remains the same with minor variations.

VES data with random noise

Figure 4(a) shows the match between a synthetic Q-type VES curve (⊛) with 10% Gaussian random noise added to each data sample and the computed curve (○). The final VFSA model (Fig. 4b) shows that the thicknesses of the layers are the same as those of the model and that the variations in the resistivities of the layers from the true model, shown in parentheses, are nominal only. The histograms (Fig. 5) show that all the parameters, i.e. ρ_1, ρ_3, h_1 and h_2, except ρ_2, are very well resolved. The resolution of ρ_2 is also good. The *a posteriori* correlation matrix (Fig. 6) shows that there is a negative correlation between ρ_2 and h_1, which means that if the estimated value of ρ_2 is in error with respect to the true unknown value, then it is almost certain that the estimated value for h_1 will also be in error because the absolute value of correlation is close to 1, and the sign of the error will be opposite to that of the error

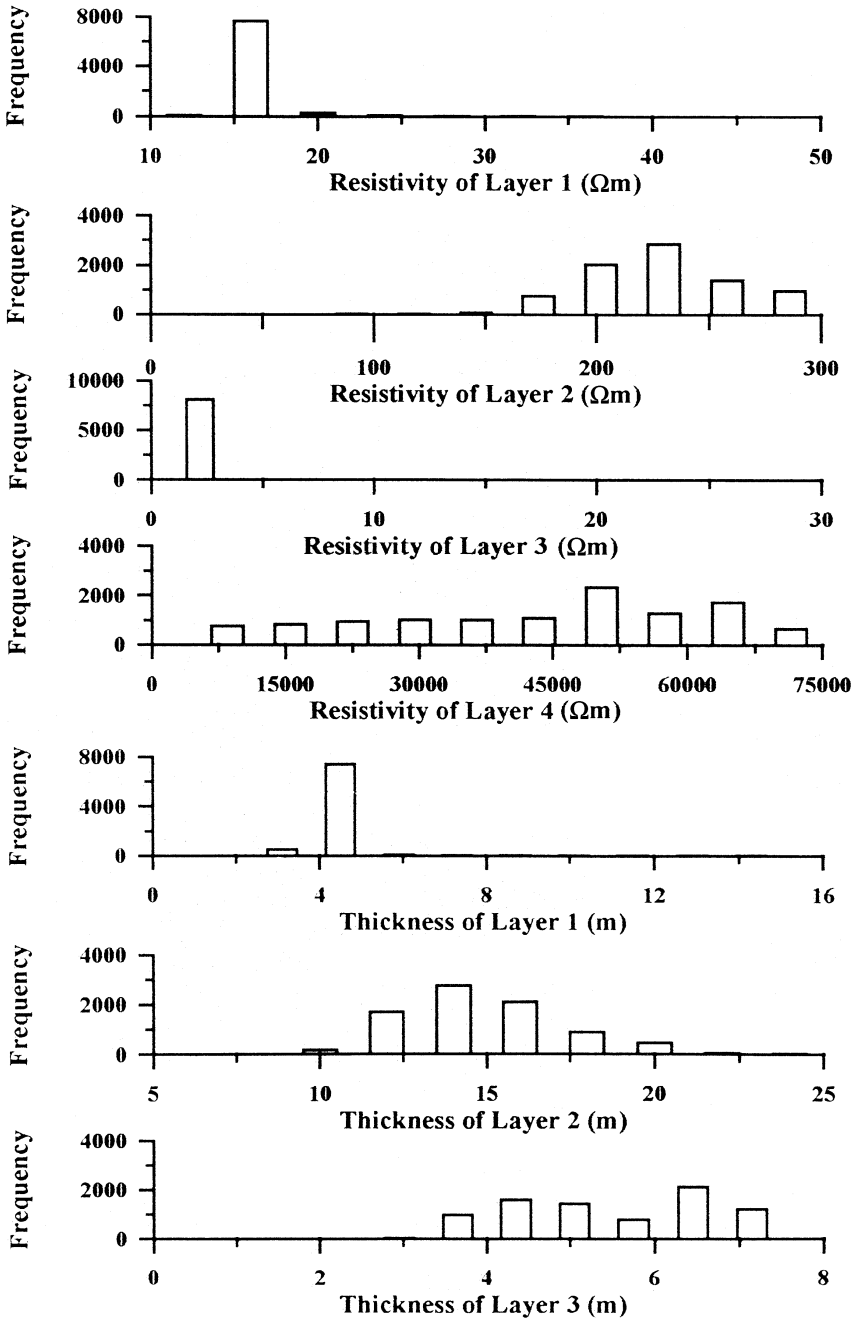

Figure 11 Histograms of the model parameters of the field VES curve for VFSA inversion (Fig. 10), sampled at 10 000 iterations.

in the estimated value of ρ_1 because the correlation is negative (Tarantola 1987).

IP sounding data

Figures 7, 8 and 9 show the synthetic IP curve, histograms and correlation matrix, respectively. The match between the synthetic (⋇) and computed (○) curves is shown in Fig. 7(a). The final VFSA model is shown in Fig. 7(b), while the interpreted model parameters are shown in Fig. 7(c). The histograms (Fig. 8) show that ρ_1, ρ_3, m_1, m_3 and h_1 are very well resolved, and ρ_2, m_2 and h_2 are also well resolved but not to the same extent. The *a posteriori* correlation matrix (Fig. 9) in this case shows negative correlation between ρ_1 and h_1, ρ_3 and m_3, and m_2 and h_2. It also shows negative correlation between ρ_1 and m_2, and h_1 and h_2. There is positive correlation between

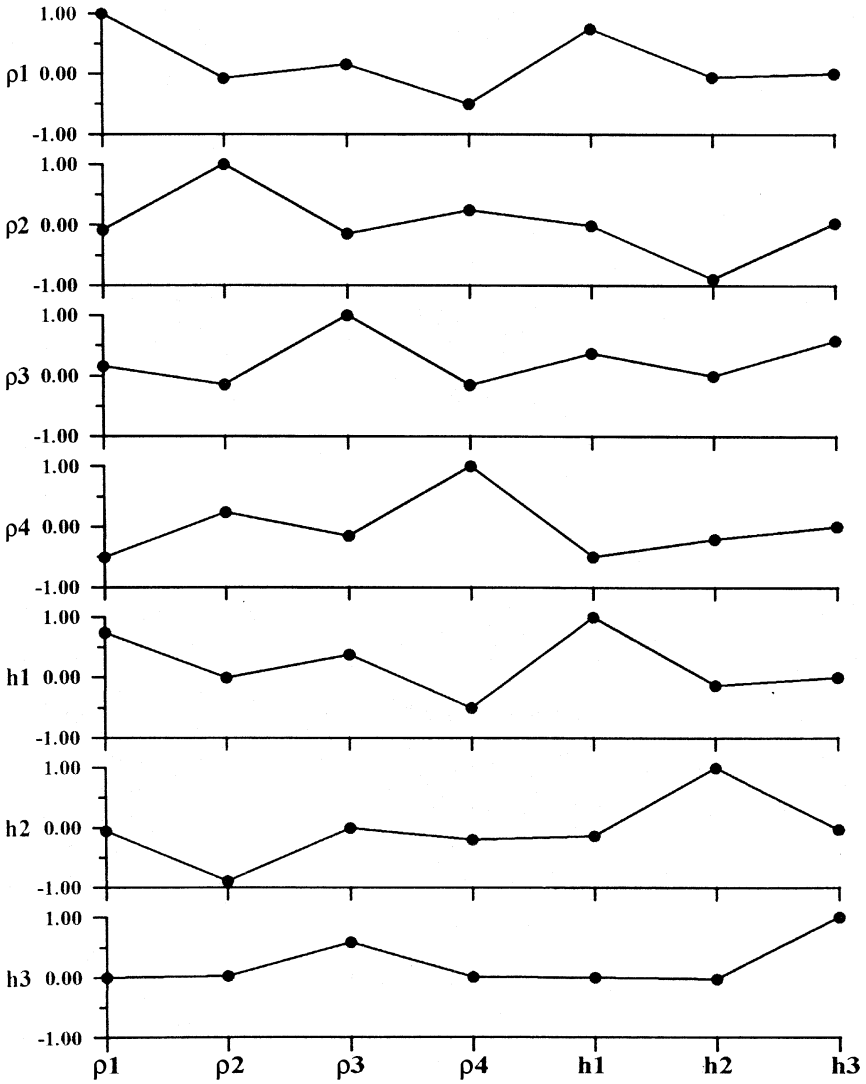

Figure 12 *A posteriori* correlation matrix for the field VES curve (Fig. 10).

m_2 and h_1. Positive correlation between the parameters means that if the parameters are changed, such that the ratios of the parameters are the same, then the sounding curve will remain unchanged, whereas negative correlation between the parameters means that if the parameters are changed, such that the product of the parameters are the same, then the sounding curve will also remain unchanged. Thus, the correlation matrix always indicates those combinations of the original parameters that least affect the sounding curve (Inman 1975).

Field VES and IP sounding data

Here we present the sensitivity and resolution analysis of a four-layer field curve for groundwater exploration and a four-layer IP curve for mineral exploration.

VES data

VES curves with a Schlumberger array were acquired for a groundwater survey in an area where a granitic basement is overlain by lava flows (trap) in the Medak district, Andhra Pradesh, India (Reddy, Murty and Kesavamani 1990). Some of the boreholes drilled on the basis of VES surveys in this drought-prone area yield 20 000–25 000 l of groundwater per minute. The VES curve shown by asterisks (⋇) in Fig. 10(a) is a four-layer case of KH-type. The search window and search increments are shown in Table 2. The computed values from the VFSA inversion are represented by open circles (○). The lithology of the borehole as obtained from the driller's log gives the following thicknesses for the layers: top soil cover = 5.6 m; trap = 16.4 m; clay = 5.5 m. The basement is granite. The resistivity log from the borehole is not available. The sections

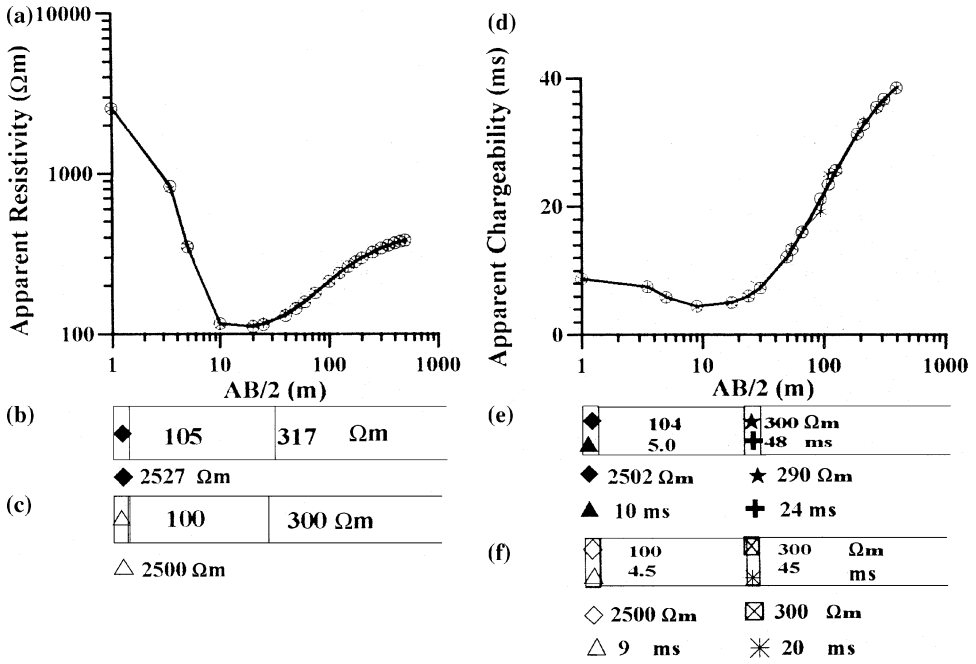

Figure 13 (a) Field (✳) and computed (○) ρ_a^* curves; (b) VFSA model; (c) subsurface resistivity model reproduced from Dixon and Doherty (1977); (d) field (✳) and computed (○) IP curves; (e) VFSA model; (f) subsurface IP model reproduced from Dixon and Doherty (1977).

below Fig. 10(a) show the final VFSA model (Fig. 10b) and the borehole log (Fig. 10c). Histograms of the model parameters sampled over 10 000 iterations are shown in Fig. 11. The values of ρ_1, ρ_3 and h_1 are very well resolved. The larger spread of the histograms for ρ_2, ρ_4, h_2 and h_3 show that these parameters are not very well resolved. A plot of the *a posteriori* correlation matrix is shown in Fig. 12. It should be noted that there is a strong negative correlation between ρ_2 and h_2 where the resistivity is relatively high. There is a positive correlation between ρ_3 and h_3, where the resistivity is relatively low. This is consistent with observations reported by Jupp and Vozoff (1975) and Vozoff and Jupp (1975). The histograms for ρ_2, h_2 and h_3 show a large spread.

Table 2 Search window and search increments for the layer parameters of the field VES curve

Layers	ρ_{min} (Ωm)	ρ_{max} (Ωm)	$\Delta\rho$ (Ωm)	h_{min} (m)	h_{max} (m)	Δh (m)
1	10	50	2	1	15	1
2	20	300	5	5	25	1
3	1	25	1	0.5	7.5	0.5
4	5000	750 000	1000	–	–	–

IP sounding data

We now consider an interesting field case carried out on Mt. Turner, North Queensland, Australia, taken from Dixon and Doherty (1977). It is known that anomalous regions of high or low conductivity do not necessarily correspond to regions of high chargeability. This example has been specifically selected to show that IP gives additional information about the subsurface structure. In this case, the resistivity sounding of a three-layer earth (Fig. 13c) appears as a four-layer earth in the IP sounding curve (Fig. 13f) due to the presence of a polarizable layer at the top of the bottommost layer, and this polarizable layer does not show any significant difference in resistivity from the underlying layer. The matches of apparent resistivity and apparent chargeability curves using the final VFSA model are shown in Figs 13(a) and 13(d), respectively. The final VFSA models are shown in Figs 13(b) and 13(e). The corresponding subsurface models near Mt. Turner, North Queensland, presented by Dixon and Doherty (1977), are reproduced in Figs 13(c) and 13(f). Figure 14 shows the histograms of the model parameters sampled over 10 000 iterations. The layer parameters, ρ_1, ρ_2, ρ_4, h_1, h_2, h_3 and m_1, are well resolved, but not ρ_3, m_2 and m_3. The *a posteriori* correlation matrix is shown in Fig. 15. There is no correlation between the layer parameters.

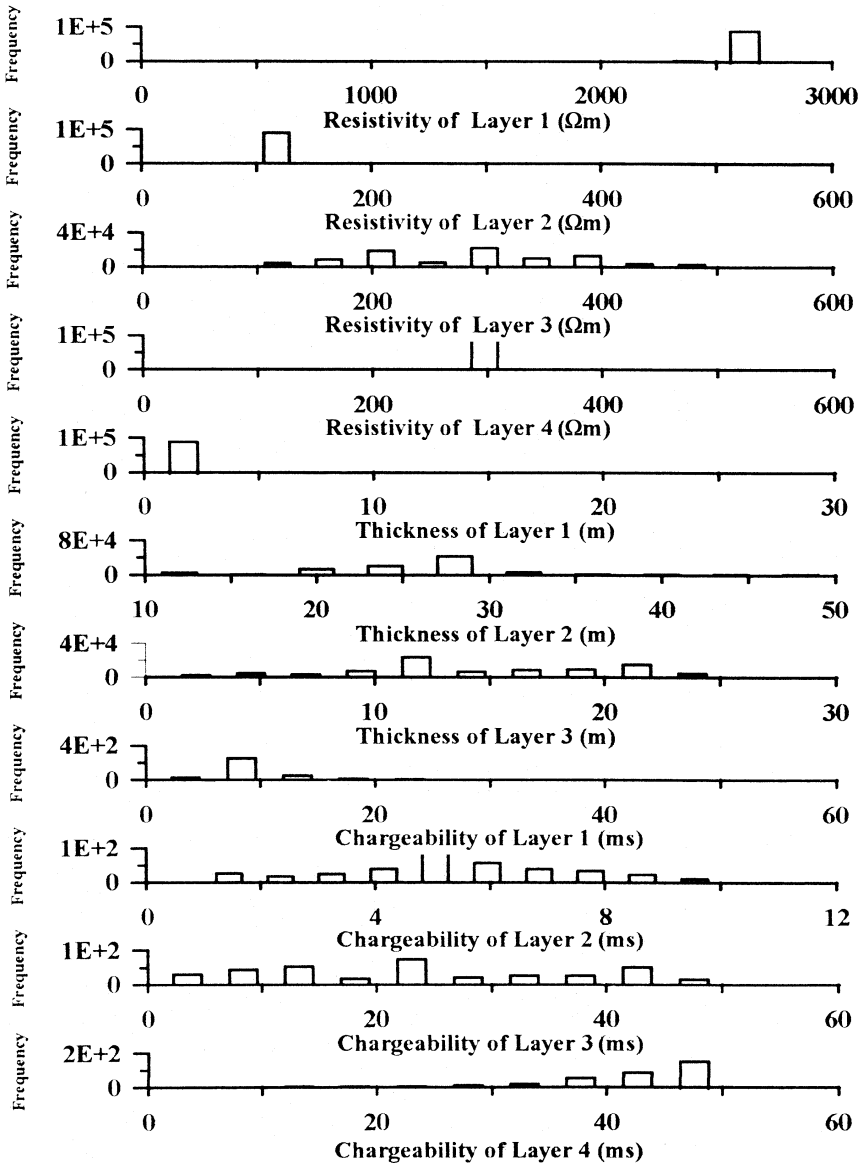

Figure 14 Histograms of the model parameters of the field IP curve for VFSA inversion (Fig. 13d), sampled at 10 000 iterations.

CONCLUSIONS

We have demonstrated the use of the VFSA method, which is a variant of SA, for resolution, sensitivity and uncertainty analysis in the inversion of 1D DC resistivity and IP sounding data. The non-linear inversion does not require a good starting model and has been found to be successful in inversion of resistivity and IP sounding data. The method has been validated using several synthetic models as well as field data. The final values of the parameters are in agreement with the borehole data. The resolution capability of the VFSA algorithm is also satisfactory, as shown by the sensitivity analysis. It takes about 5 minutes on a PC 486 (66 MHz; 16 Mb RAM) to carry out 10 000 iterations. The VFSA thus can be used for routine interpretation of VES and IP sounding data, incorporating resolution, sensitivity and uncertainty of layer parameters to make the interpretation more meaningful.

ACKNOWLEDGEMENTS

We are grateful to Dr B. Banerjee, Senior Director, Marine Wing, GSI (ER), Dr Ranjit K. Shaw, Department of Applied Geophysics, Indian School of Mines (ISM), Dhanbad, and Manoj K. Singh, Junior Research Fellow (JRF), Mining

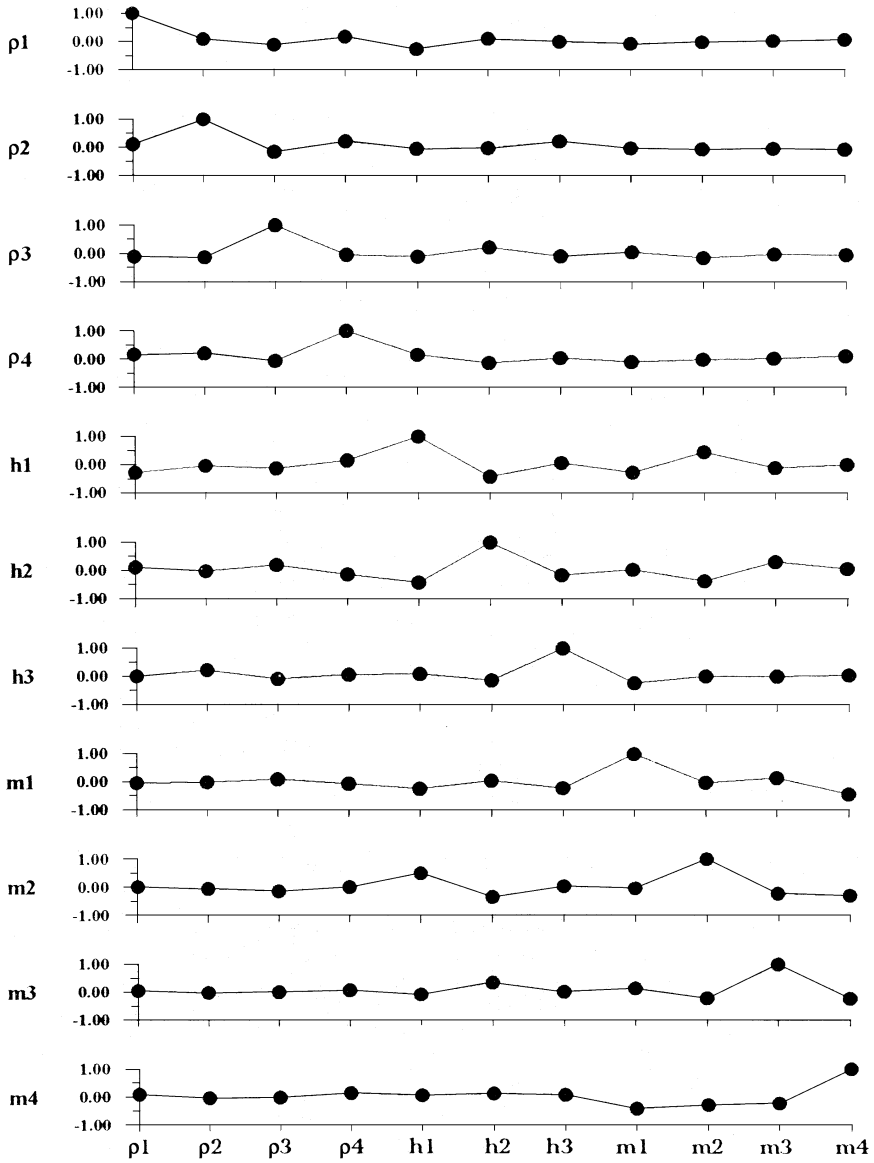

Figure 15 *A posteriori* correlation matrix for the field IP curve (Fig. 13d).

Engineering Department, ISM Dhanbad, for useful discussions and advice. We also thank Rajib K. Sinharay, JRF, Department of Applied Geophysics (AGP), ISM, for helpful comments. The computations were carried out in the computer centre of UGC SAP DSA of AGP, ISM, Dhanbad.

REFERENCES

Barker R.D. 1990. Investigations of groundwater salinity by geophysical methods. In: *Geotechnical and Environmental Geophysics*: Investigations in Geophysics No. 5, **2** (ed. S.H. Ward), pp. 201–211. Society of Exploration Geophysicists.

Beard L.P. and Hohmann G.W. 1992. Subsurface imaging using approximate IP inversion. 62nd SEG Meeting, New Orleans, USA, Expanded Abstracts, 427–430.

Beard L.P., Hohmann G.W. and Tripp A.C. 1996. Fast resistivity/IP inversion using a low contrast approximation. *Geophysics* **61,** 169–179.

Bertin J. and Loeb J. 1976. *Experimental and Theoretical Aspects of Induced Polarization* **1** and **2**. Gebrüder Borntraeger.

Bhattacharya B.B. and Ghosh Roy I. 1988. A method of inversion and its application to VES measurements. In: *Advances in Geophysics* (ed. B.B. Bhattacharya), pp. 43–64. Oxford and IBH Publishing Co.

Chunduru R.K., Sen M.K. and Stoffa P.L. 1996. 2-D resistivity inversion using spline parameterization and simulated annealing. *Geophysics* **61,** 151–161.

Chunduru R.K., Sen M.K., Stoffa P.L. and Nagendra R. 1995. Non-linear inversion of resistivity profiling data for some regular geometrical bodies. *Geophysical Prospecting* **43,** 979–1003.

Dixon O. and Doherty J.E. 1977. New interpretation methods for IP soundings. *Australian Society of Exploration Geophysicists* **8,** 65–69.

Esparza F.J. and Gomez-Trevino E. 1997. 1-D inversion of resistivity and induced polarization data for the least number of layers. *Geophysics* **62,** 1724–1729.

Fink J.B., McAlister E.O., Sternberg B.B., Wieduwilt W.G. and Ward S.H. (eds) 1990. Induced polarization. In: *Applications and Case Histories:* Investigations in Geophysics No. 4, p. 410. Society of Exploration Geophysicists.

Ghosh D.P. 1970. *The application of linear filter theory to the direct interpretation of geoelectric resistivity measurements*. PhD thesis, Technical University of Delft.

Ghosh D.P. 1971a. The application of linear filter theory to the direct interpretation of geoelectric sounding measurements. *Geophysical Prospecting* **19,** 192–217.

Ghosh D.P. 1971b. Inverse filter coefficients for the computation of apparent resistivity standard curves for a horizontally stratified earth. *Geophysical Prospecting* **19,** 769–775.

Hohmann G.W. and Raiche A.P. 1987. Inversion of controlled source electromagnetic data. In: *Electromagnetic Methods in Applied Geophysics* **1**: Investigations in Geophysics No. 3 (ed. M.N. Nabighian), pp. 469–503. Society of Exploration Geophysicists.

Ingber L. 1989. Very fast simulated reannealing. *Mathematical and Computer Modelling* **12,** 967–993.

Ingber L. and Rosen B. 1992. Genetic algorithms and very fast simulated reannealing: a comparison. *Mathematical and Computer Modelling* **16,** 87–100.

Inman J.R. 1975. Resistivity inversion with ridge regression. *Geophysics* **40,** 798–817.

Inman J.R., Ryu J. and Ward S.H. 1973. Resistivity inversion. *Geophysics* **38,** 1088–1108.

Jenkins G.M. and Watts D.G. 1968. *Spectral Analysis and its Applications*. San Holden-Dai, Inc.

Jupp D.L.B. and Vozoff K. 1975. Stable iterative methods for the inversion of geophysical data. *Geophysical Journal of the Royal Astronomical Society* **42,** 957–976.

Koefoed O. 1979. *Geosounding Principles* **1**: *Resistivity Sounding Measurements*. Elsevier Science Publishing Co.

La Brecque D.J. 1991. IP tomography. 61st SEG Meeting, Houston, USA, Expanded Abstracts, 413–416.

Menke W. 1984. *Geophysical Data Analysis: Discrete Inverse Theory*. Academic Press, Inc.

Metropolis N., Rosenbluth A., Rosenbluth M., Teller A. and Teller E. 1953. Equation of state calculations by fast computing machines. *Journal of Chemical Physics* **21,** 1081–1092.

Mosegaard K.E. and Tarantola A. 1995. Monte Carlo sampling of solutions to inverse problems. *Journal of Geophysical Research* **B7,** 12431–12447.

Narayan S. and Dusseault M.B. 1992. Resistivity inversion method applied to shallow structural problems. *Geotechnique et Informatique* [further details not available].

Narayan S., Dusseault M.B. and Nobes D.C. 1994. Inversion techniques applied to resistivity inverse problems. *Journal of Inverse Problems* **10,** 669–686.

Normark E. and Mosegaard K. 1993. Residual statics estimation: scaling temperature schedules using simulated annealing. *Geophysical Prospecting* **41,** 565–578.

Oldenburg D.W. and Li Y. 1994. Inversion of induced polarization. *Geophysics* **59,** 1327–1341.

Oldenburg D.W., Li Y. and Ellis R.G. 1997. Inversion of geophysical data over a copper gold porphyry deposit: a case history for Mt. Milligan. *Geophysics* **62,** 1419–1431.

Patella D. 1975. A numerical computation procedure for the direct interpretation of geoelectric sounding. *Geophysical Prospecting* **23,** 335–362.

Patra H.P. and Nath S.K. 1998. *Schlumberger Geoelectric Sounding in Groundwater (Principles, Interpretation and Application)*. Oxford and IBH Publishing Co., Pvt. Ltd, New Delhi/A.A. Balkema, Rotterdam.

Pelton W.H., Rijo L. and Swift C.M. 1978. Inversion of two dimensional resistivity and induced polarization data. *Geophysics* **43,** 788–803.

Reddy A.G.B., Murty B.S.R. and Kesavamani M. 1990. *A Compendium of Four Decades of Geophysical Activity in GSI*. Geological Survey of India.

Rijo L. 1984. Inversion of 3-D resistivity and induced polarization data. 54th SEG Meeting, Atlanta, USA, Expanded Abstracts, 113–117.

Rothman D.H. 1985. Nonlinear inversion, statistical mechanics, and residual statics estimation. *Geophysics* **50,** 2784–2796.

Sasaki Y. 1982. Automatic interpretation of induced polarization data over two-dimensional structures. *Memoirs of the Faculty of Engineering of Kyushu University* **42,** 59–74.

Seigel H.O. 1959. Mathematical formulation and type curves for induced polarization. *Geophysics* **24,** 547–565.

Sen M.K., Bhattacharya B.B. and Stoffa P.L. 1993. Nonlinear inversion of resistivity sounding data. *Geophysics* **58,** 496–507.

Sen M.K. and Stoffa P.L. 1991. Nonlinear one-dimensional seismic waveform inversion using simulated annealing. *Geophysics* **56,** 1624–1638.

Sen M.K. and Stoffa P.L. 1995. *Global Optimization Methods in Geophysical Inversion*. Elsevier Science Publishing Co.

Shima H. 1990. Two-dimensional automatic resistivity inversion technique using alpha centres. *Geophysics* **55,** 682–684.

Sumner J.S. 1976. *Principles of Induced Polarization for Geophysical Exploration*. Elsevier Science Publishing Co.

Tarantola A. 1987. *Inverse Problem Theory: Methods for Data Fitting and Model Parameter Estimation*. Elsevier Science Publishing Co.

Tripp A.C., Hohmann G.W. and Swift C.M. 1984. Two-dimensional resistivity inversion. *Geophysics* **49,** 1708–1717.

Vozoff K. and Jupp D.L.B. 1975. Joint inversion of geophysical data. *Geophysical Journal of the Royal Astronomical Society* **42,** 977–991.

Ward S.H. (ed.) 1990. *Geotechnical and Environmental Geophysics: Investigations in Geophysics* No. 5, **1–3**. Society of Exploration Geophysicists.